

## **Shear Stress Estimates for Combined Wave Overtopping and Surge Overflow at an Earthen Levee**

Steven A. Hughes<sup>1</sup>, Justin M. Shaw<sup>2</sup>, and Isaac L. Howard<sup>3</sup>

<sup>1</sup>Senior Research Engineer, Coastal and Hydraulic Laboratory, U.S. Army Engineer Research and Development Center, 3909 Halls Ferry Road, Vicksburg, Mississippi 39180.

<sup>2</sup>Engineer, C. H. Fenstermaker and Associates Inc., Lafayette, LA 70508

<sup>3</sup>Assistant Professor, Department of Civil and Environmental Engineering, Mississippi State University, Mississippi State, MS 39762

### **ABSTRACT**

Twenty-seven small-scale laboratory experiments simulating combined wave overtopping and storm surge overflow on a trapezoidal levee were conducted at a prototype-to-model scale of  $N_L = 25$ . Time series measurements of irregular and unsteady flow thickness and velocity were acquired at two locations on the landward-side 1V-on-3H slope. These measurements were used to calculate the time series of instantaneous shear stress representing the average over a 4.8-m-length (prototype scale) of levee slope between the two measurement locations. An empirical relationship is presented for estimating the mean shear stress for combined wave and surge overtopping, and additional formulas are given for estimating representative parameters of the irregular shear stress peaks associated with individual overtopping waves.

### **INTRODUCTION**

Earthen levees are used throughout the world to protect communities and resources from elevated water levels in coastal and inland areas. Ideally, all levees would have a crest elevation with ample freeboard to prevent wave and/or surge overtopping for any conceivable storm scenario. However, economics dictate more practical levee designs having lower crest elevations, but with the risk that some wave/surge overtopping will occur during extreme events. One of the most prevalent levee failure modes is rapid erosion of the landward-side levee soil during overtopping events.

Overtopping on a trapezoidal levee cross section resulting from steady overflow combined with wave overtopping is an unsteady flow with large velocities and flow thicknesses at the leading edge of the overtopping wave, followed by a gradual decrease in velocity and flow thickness as the wave passes over the levee. Between waves, the landward-side slope of the levee often goes “dry” as the wave trough temporarily draws the elevated water level on the seaward side of the levee lower than the levee crest elevation. For most levees the landward-side slope is steep enough to assure the unsteady overtopping flow is supercritical.

This paper presents new small-scale laboratory measurements of combined wave overtopping and surge overflow of earthen levees with the purpose of characterizing the shear stresses induced on the landward side of the levee. Estimates of shear stress exerted by the unsteady overtopping flow would be useful for evaluating levee soil erosion potential and for designing alternative slope protection that can resist the high shear stresses during overtopping. For example, it may be possible to design temporary slope protection intended for rapid deployment prior to overtopping from severe events such as hurricanes.

#### **PREVIOUS RESEARCH ON COMBINED OVERTOPPING AND SHEAR STRESS**

Earlier research on wave overtopping of dike and levees was mostly based on physical model experiments conducted at small and large scale, and the experiments were restricted almost entirely to the case of wave-only overtopping. A good summary of presently accepted methodologies and empirical equations for estimating wave-only overtopping of levees and dikes is given in Pullen, et al. (2007). More recently, phase-resolving numerical models (Boussinesq and Reynolds Averaged Navier-Stokes) have been successfully applied to the problem of unsteady overtopping flows caused by wave-only and even combined wave and surge overtopping. For example, see Reeve, et al. (2008), Losada, et al. (2008), and Lynett, et al. (2010). Finally, the recent field work using the Dutch Wave Overtopping Simulator (van der Meer, et al. 2006, van der Meer, et al. 2008, and van der Meer, et al. 2010) has helped researchers understand levee grass cover response to sustained wave overtopping.

The earliest examination of the combined wave and surge overtopping case appears to be a study by Gibson (1930). His work focused on the effect of wind-generated surface waves on the accuracy of flow measurements made using sharp-crested and broad-crested weirs. Gibson’s research considered relatively small waves with lengths on the order of 1 m and wave heights in the range of 5 – 10 cm.

Schüttrumpf (2001) and Schüttrumpf, et al. (2001) gave equations for dimensionless average wave overtopping discharge based on laboratory experiments with zero freeboard. The equations shown below (Eqns. 1 and 2) from the Overtopping Manual (Pullen, et al. 2007) are a slightly revised version of Schüttrumpf's equations.

$$\frac{q_w}{\sqrt{g} H_{m0}^3} = 0.0537 \cdot \xi_{om-1,0} \quad \text{for } \xi_{om-1,0} < 2 \quad (\text{breaking waves}) \quad (1)$$

$$\frac{q_w}{\sqrt{g} H_{m0}^3} = \left( 0.136 - \frac{0.226}{\xi_{om-1,0}^3} \right) \quad \text{for } \xi_{om-1,0} \geq 2 \quad (\text{nonbreaking waves}) \quad (2)$$

In Eqns. 1 and 2,  $q_w$  is average overtopping discharge,  $g$  is gravitational acceleration,  $H_{m0}$  is the energy-based significant wave height, and  $\xi_{om-1,0}$  is the Iribarren number given by

$$\xi_{om-1,0} = \frac{\tan \alpha}{\sqrt{H_{m0} / L_{om-1,0}}} \quad (3)$$

with

$$L_{om-1,0} = \frac{g}{2\pi} T_{m-1,0}^2 \quad (4)$$

with  $\alpha$  being the angle from horizontal of the seaward-side slope, and  $T_{m-1,0}$  is the mean spectral energy wave period.

Pullen, et al. (2007) proposed calculating combined wave and surge overtopping discharge by superposition of surge discharge given by the broad-crested weir formula and wave discharge at zero freeboard (Eqn. 1 or 2). For example, the combined overtopping discharge ( $q_{ws}$ ) for breaking waves with  $\xi_{om-1,0} < 2$  would be the following:

$$q_{ws} = q_{surge} + q_{wave} = 0.6 \sqrt{g} | -R_c |^{3/2} + 0.0537 \cdot \xi_{om-1,0} \sqrt{g} H_{m0}^3 \quad (5)$$

where  $R_c$  is the freeboard. The freeboard will be negative for this case, and it must be entered as a negative number to avoid producing a complex number for the result. In the EurOtop Manual (Pullen, et al. 2007) a coefficient of 0.6 was used in the broad-crested weir formula

rather than the more customary 0.5443. Equation 5 was acknowledged as being tentative until such time that supporting experimental data could be collected.

Hughes and Nadal (2009) developed a discharge relationship for combined wave overtopping and surge overflow under a variety of flow conditions using a small-scale levee physical model. The test facility and levee model was the same physical model set-up used for the study described in this paper, and complete details of the physical model are presented in Hughes (2008) and Hughes, et al. (2011). Hughes and Nadal (2009) measured flow depth and velocity at on the levee crest at the co-located pressure gauge and LDV, and they calculated discharge as the product of depth and velocity. The measurements gave a trend of increasing dimensionless discharge with increasing relative freeboard given by the best-fit empirical equation

$$\frac{q_{ws}}{\sqrt{g} H_{m0}^3} = 0.034 + 0.53 \left( \frac{-R_c}{H_{m0}} \right)^{1.58} \quad ; \quad R_c < 0 \quad (6)$$

Hughes and Nadal (2009) also presented empirical equations for distribution of instantaneous discharge and distribution of individual overtopping wave volumes. On the landward-side slope, the following equations were given for estimating mean flow thickness ( $h_m$ ), mean velocity ( $v_m$ ), and root-mean-squared of the peak flow thickness ( $h_{rms}$ ).

$$h_m = 0.4 \left[ \frac{1}{g \sin \theta} \right]^{1/3} (q_{ws})^{2/3} \quad (7)$$

$$v_m = 2.5 (q_{ws} \cdot g \cdot \sin \theta)^{1/3} \quad (8)$$

$$\frac{h_{rms}}{h_m} = 1 + 0.0077 \left( \frac{g H_{m0} T_p}{q_{ws}} \right)^{2/3} \quad (9)$$

In Eqns. 7–9,  $\theta$  is the angle from horizontal of the landward-side levee slope, and  $T_p$  is the peak spectral wave period. Hughes and Nadal stated that Eqns. 7–9 are only applicable to landward slopes of 1V:3H with a small friction factor.

Estimation of shear stress on the landward-side levee slope due to unsteady, non-uniform overtopping flow requires synoptic time series of slope-perpendicular flow depth and slope-

parallel flow velocity at two down-slope locations to evaluate flow accelerations. Nadal and Hughes (2009) and Hughes and Nadal (2010) estimated overtopping shear stresses for combined wave overtopping and surge overflow based on measurements reported in Hughes and Nadal (2009). They had synoptic measurements of flow thickness at two locations on the levee slope, but they only had velocity measurements at one of the locations. The velocity time series at the second location was synthesized based on the hypothesis that the time series of instantaneous discharge was the same at both locations with the only difference being a short time lag. They shifted the discharge time series from the first location to the second location, and then calculated the corresponding velocity time series at the second location as the discharge divided by the flow thickness, i.e.,  $v(t) = q(t) / h(t)$ . Additional details of this procedure are given in Nadal and Hughes (2009). The hypothesis that the discharge time series is conserved along the levee landward-side slope was later proven as reported by Hughes and Shaw (2011).

Hughes and Nadal (2010) calculated the shear stress time series for each of the 27 experiments, and they presented an empirical relationship between the hydrodynamic parameters and the corresponding mean shear stresses estimated from the synthesized shear stress time series. The best best-fit of the data was a simple expression relating the mean shear stress to the specific weight of (fresh) water,  $\gamma_w$ , and the root-mean-square of the peak flow thicknesses perpendicular to the levee slope,  $h_{rms}$ , i.e.,

$$\tau_{0,mean} = 0.235 \gamma_w h_{rms} \quad (10)$$

They noted that Eqn. 10 applies only to smooth slopes having similar frictional resistance as the levee model used in the tests, and the equation may only apply for the same 1V:3H landward-side slope.

The mean shear stress values estimated by Eqn. 10 provide an overall average that occurs during a combined wave and surge overtopping event. However, in the time series of instantaneous shear stress acting on the landward-side slope, the peak stresses associated with the overtopping wave crests can be several times the magnitude of the mean shear stress. The peak shear stress acts for a short duration as the wave passes down the slope, but the peak shear stress may well be the defining parameter with respect to stability of armoring alternatives or for determining rates of soil erosion.

Nadal and Hughes (2009) analyzed the calculated time series of instantaneous shear stress in the time domain using standard up-crossing analysis. The maximum shear stress values for each identified wave were rank-ordered, and representative values were determined for the average of the highest 1/3, highest 1/10, and highest 1/100 of the peak shear stresses. These values were denoted as  $\tau_{p,1/3}$ ,  $\tau_{p,1/10}$ , and  $\tau_{p,1/100}$ , respectively. Good correlations were found between the representative peak shear stresses and the product of specific weight of water,  $\gamma_w$ , and a representative measure of flow depth given by the root-mean-square overtopping wave height on the landward-side levee slope,  $H_{rms}$ , which is slightly different than the root-mean-square of the peak flow thicknesses,  $h_{rms}$ .

$$\tau_{p,1/3} = 0.53 \gamma_w H_{rms} \quad (11)$$

$$\tau_{p,1/10} = 0.69 \gamma_w H_{rms} \quad (12)$$

$$\tau_{p,1/100} = 0.93 \gamma_w H_{rms} \quad (13)$$

where

$$\frac{H_{rms}}{h_m} = 3.43 \cdot \exp\left(\frac{R_c}{H_{m0}}\right) \quad (14)$$

In Eqn. 14 the value of negative freeboard must be entered as a negative number. The mean flow thickness is estimated from Eqn. 7. Based on relatively good fit of the data, Nadal and Hughes (2009) concluded that Eqns. 11–14 provide a reasonable estimate for the more extreme shear stresses that can occur on levee slopes having relatively smooth surfaces.

Estimates of shear stress on the landward-side slope resulting from steady overflow were made by Briaud, et al. (2008). A Reynolds-averaged Navier-Stokes (CHEN3D) numerical model was used to estimate steady overflow on a levee with a 5-m crest and 1V:5H landward-side and seaward-side slopes. The water free surface had an elevation 1 m above the levee crest (i.e.,  $R_c = -1$  m). Model forcing was by a 3-m/s horizontal current imposed on the upstream boundary in addition to gravity flow down the landward-side slope. The numerical model estimated a maximum velocity of 11.8 m/s near the landward-side levee toe, and maximum shear stresses at the toe were stated to be between 50 and 60 N/m<sup>2</sup>. These

computed shear stresses are nearly an order of magnitude smaller than calculated by Nadal and Hughes (2009) for similar flows using measured data from small-scale experiments.

The validity of Briaud, et al.'s (2008) shear stress estimates was examined by Hughes, et al. (2011) using the widely-accepted equations for steady overflow discharge and shear stress at terminal velocity on a slope. The steady overflow discharge corresponding to a negative freeboard of  $R_c = -1.0$  m was estimated using the broad-crested weir formula (see Eqn. 15) as follows.

$$q_s = 0.5443 \sqrt{g} (-R_c)^{3/2} = 0.5443 \sqrt{9.816 \text{ m/s}^2} [ -(-1.0 \text{ m}) ]^{3/2} = 1.7 \text{ m}^3/\text{s per m}$$

Next, at the landward-side toe of the levee with a computed velocity of  $v = 11.8$  m/s, the estimated steady flow thickness was found from mass continuity simply as

$$h = \frac{q_s}{v} = \frac{1.7 \text{ m}^3/\text{s/m}}{11.8 \text{ m/s}} = 0.14 \text{ m}$$

Finally, the shear stress on the slope created by the flowing water was estimated from the shear stress equation for steady flow. At terminal velocity the friction slope  $S_f$  is replaced with  $S_o = \sin \theta = \sin (11.3 \text{ deg})$ , and the estimated shear stress (see Eqn. 18) is found to be the following.

$$\tau_o = \gamma_w h S_f = (10 \text{ kN/m}^3)(0.14 \text{ m}) \sin(11.3^\circ) = 0.275 \text{ kN/m}^2 = 275 \text{ N/m}^2$$

Thus, this simple approximation of shear stress using established empirical equations produces shear stress estimates that are between 4 and 5 times greater than the shear stresses computed by Briaud, et al.'s (2008) numerical model simulation.

## **EXPERIMENT DESCRIPTION**

Measurements of instantaneous flow parameters necessary to estimate the hydrodynamic shear stress were acquired during laboratory tests that simulated combined storm surge overflow and wave overtopping of a levee with a trapezoidal cross section. The study was conducted in a two-dimensional laboratory flow/wave flume at a nominal prototype-to-model length scale of 25-to-1 ( $N_L = 25$ ). Small-scale hydrodynamic laboratory experiments raise concerns about scale effects that might influence model results and lead to inaccurate

representation of real-world flow behavior. Hughes and Shaw (2011) presented results that used the same test facility and hydrodynamic conditions, and they discussed potential scale effects. The main identified scale effect was lack of air entrainment during overtopping in the small-scale model compared to the considerable air entrainment at full-scale. They concluded that the consequences of this scale effect have not yet been resolved, but they were optimistic that the small-scale measurements were reasonable predictors of the macro features of full-scale flow behavior. See Hughes and Shaw (2011) for further details.

## **Facility**

The experiments were conducted in a 0.9-m-wide wave flume at the U.S. Army Engineer Research and Development Center (ERDC), Coastal and Hydraulics Laboratory (CHL) in Vicksburg, Mississippi. The tested levee cross section replicated in the physical model is shown in Figure 1. Surge and waves that overtopped the levee flowed into the reservoir, and a pump recirculated the water to the seaward end of the flume. Further description of the flume and details of wave generation and operating procedures can be found in Hughes (2008) and Hughes and Nadal (2009).

## **Measurements**

Time series of flow depth at two locations on the levee crown and flow thickness at five locations on the landward-side slope were measured using pressure cells embedded in the model levee. Figure 2 shows the pressure sensor locations. Time series of flow velocity were collected using laser Doppler velocimeters (LDVs) positioned at pressure gauge locations P4 and P7 as indicated by the dots in Figure 2. At these locations the LDV beam crossing points were on a line perpendicular to the levee slope and centered on the pressure sensor. The LDVs were oriented to measure slope-parallel velocity at positions that were generally half of the steady overflow thickness. The exceptions were tests with the lowest steady overflow. In these cases, the flow thickness for steady overflow was quite thin, so the LDV beams were moved closer to the upper limit of the flow thickness, or even slightly above the steady flow water surface. Figure 3 shows a photograph of the experiment set up.

As noted by Hughes and Shaw (2011), the drawback to placing the LDV beams at mid-flow thickness or above was the loss of velocity signal during wave troughs when the water level fell below the elevation of the laser beams. The instantaneous discharge over the levee at each time step was estimated at locations P4 and P7 as the product of horizontal velocity and

water depth. Incident wave characteristics were measured at a three-gauge array located seaward of the model levee.

For the shear stress tests the prototype-scale target wave conditions were the same as those used in previous tests described by Hughes (2008) and Hughes and Nadal (2009). Nine combinations of wave height and peak period ( $H_{m0} = 0.9, 1.8, \text{ and } 2.7 \text{ m}$ ; and  $T_p = 6, 10, \text{ and } 14 \text{ sec}$ ) were simulated in the model at 3 different negative freeboards ( $R_c = -0.3, -0.9, \text{ and } -1.5 \text{ m}$ ), giving a total of 27 distinct hydrodynamic conditions. Previously synthesized, scaled, and calibrated piston-type wave board displacement time series were used in the experiments to generate waves fitting the spectral parameters.

## **DATA COLLECTION, PROCESSING AND ANALYSIS**

### **Data Collection**

Data collection was completed in the same manner as described in Hughes and Shaw (2011). Briefly, the steady overflow was adjusted to the correct level, and then the wave motion was started. Data collection started when the wave board motion began. Time series of sea surface elevation data at four wave gauges, and flow thickness at seven pressure gauges were collected at a 100-Hz rate on one system, and velocity data were collected from two interconnected Dantec FlowExplorer LDVs using a different computer system. The data from the two systems were synchronized using the procedure described in Hughes and Shaw (2011). The LDVs collected velocity data at a nonuniform rate that was quite a bit faster than 100 Hz.

Each experiment lasted for 600 seconds. This gave about 200 waves for experiments with the longest peak spectral periods, and about 280 waves for the shortest peak periods. The wave and pressure time series contained 60,000 points for each data channel, with the first 1,000 to 1,600 points recording only the steady overflow before the arrival of the first waves.

### **Data Processing**

Sea surface elevation time series from the three-gauge array closest to the model levee were analyzed for incident and reflected wave energy using the frequency-domain method of Goda and Suzuki (1976), and the results were expressed in terms of energy-based incident significant wave height,  $H_{m0}$ . MatLab<sup>®</sup> scripts were used to perform additional post-

processing of the measurements. On the steep landward-side slope, the pressure measured by gauges P3–P7 was not hydrostatic, and the slope-perpendicular flow thickness was determined as  $h = (p/\gamma_w) / \cos\theta$ , where  $\gamma_w$  is the water specific weight, and  $\theta$  is the angle from horizontal of the landward-side slope (Henderson 1966). In addition, some of the pressure channels contained obvious spikes, and a spike removal routine was implemented that removed some, but not all, of the more severe spikes. Processing of the velocity data, synchronization of the velocity and flow thickness time series, and daily adjustments to the pressure gauge zeros was exactly the same as described in Hughes and Shaw (2011). Complete details of the data post-processing are given in Hughes, et al. (2011).

### Data Analysis

The instantaneous discharge passing over the levee crest and down the landward-side slope at each time step was estimated at locations P4 and P7 on the landward-side slope as the product of horizontal velocity and water depth. These estimates assumed that velocity was parallel to the levee surface and constant throughout the water thickness at each location.

An average of the discharge between data points 100 and 1,000 was taken as the steady overflow discharge for the experiment because the first waves generated in the flume had not yet reached the levee model. An estimate of the surge elevation above the levee crest (negative freeboard) was calculated using the generally accepted equation for flow over a broad-crested weir given by open channel flow texts (e.g., Henderson 1966)

$$q_s = \left(\frac{2}{3}\right)^{3/2} \sqrt{g} (-R_c)^{3/2} = 0.5443 \sqrt{g} (-R_c)^{3/2} \quad (15)$$

where  $q_s$  is the steady overflow discharge per unit length,  $g$  is gravity, and  $R_c$  is the negative freeboard (difference between levee crest elevation and surge elevation). Average overtopping discharge,  $q_{ws}$ , due to combined wave and surge overtopping was calculated at locations P4 and P7 using data points 3,000 to 59,400 (564 seconds at 100-Hz rate) for each time series. It was assumed that the best estimate of mean discharge came from the gauges located at position P4, and that the flow thickness at location P7 should be adjusted slightly as necessary to match the total average discharge at location P4. The discharge estimates at location P7 were consistently greater than at location P4 by about 7 percent, so the flow

thicknesses at P7 were multiplied by a reduction factor of 0.94 to give a better match of total discharge. Full details are provided in Hughes, et al. (2011).

Table 1 presents the steady overflow ( $q_s$ ) and combined wave and surge overtopping discharges ( $q_{ws}$ ) per unit length at locations P4 and P7 for 25 of the 27 experiments. Runs 25 and 27 were eliminated because of unexplained measurement errors. Steady overflow was not measured for runs at the lowest negative freeboard because the LDV beams were not immersed during steady overflow. Also included in Table 1 are the resolved incident wave parameters and the negative freeboard crest calculated from Eqn. 15 using the values of  $q_s$  determined at location P4. The parameter  $T_{m-1,0}$  is the mean spectral energy wave period. All parameter values in Table 1 have been converted to prototype scale size using the prototype-to-model length scale ratio of  $N_L = 25$ .

Hughes, et al. (2011) showed that calculated values of average discharge for combined wave and surge overtopping ( $q_{ws}$ ) compared very well with predictions from Hughes and Nadal's empirical equation (Eqn. 6). The comparison did not include tests at the lowest surge level where the negative freeboard could not be determined precisely.

## RESULTS

### Mean Flow Thickness and Velocity for Combined Wave and Surge Overtopping

The mean values of discharge, flow thickness, and velocity at locations P4 and P7 for combined wave and surge overtopping were calculated from the measured time series starting at data point 3,400 and ending at data point 60,000. This 566-s portion of the time series represented a prototype-scale time of 47 min 10 s.

Measured mean flow thickness for combined wave and surge overtopping were plotted versus average overtopping discharge ( $q_{ws}$ ) on Figure 4. The solid line is Eqn. 7 suggested by Hughes and Nadel (2009). Mean flow thicknesses at location P4 are uniformly slightly less than predicted by Eqn. 7, and flow thicknesses at location P7 are considerably less than predicted. This comparison indicates that Hughes and Nadal (2009) were incorrect in assuming that small differences in flow thickness between locations P4 and P7 could be effectively represented by the average between the two. The clear distinction between measured flow thicknesses at the two locations indicates flow acceleration was still occurring, whereas the formulation of Hughes and Nadal assumed that terminal conditions had been

reached over this length of the landward-side slope. The fact that the measurements for this test series are all less than predicted can probably be ascribed to the adjustments that were made to the flow thickness time series to compensate for inaccurate zeroing of the pressure gauges. A similar adjustment was not performed by Hughes and Nadal (2009).

Figure 5 presents the mean flow velocities on the landward-side levee slope as a function of combined overtopping discharge. The solid line represents Hughes and Nadal's (2009) tentative prediction equation given by Eqn. 8. Measured mean velocities at location P4 are only slightly under-predicted by Eqn. 8, but the mean velocities at location P7 are significantly under-predicted. The difference between the measured velocities at the two locations is due to the fact that the flow was still accelerating down the slope. One factor that may be contributing to the velocity difference is the loss of lower-speed velocity data when the LDV beams are not submerged in the flow at thin flow thicknesses. Thus, the velocity average does not include some of the lower velocity data points that would decrease the means by some unknown amount. This effect would be more problematic at location P7 that experienced relatively thinner flows with the LDV beams out of the flow for longer periods.

Unlike instantaneous discharge, instantaneous flow thickness and velocity are a function of distance down the landward-side slope until terminal flow conditions are reached for all values. For this reason it is difficult to develop reliable empirical estimators of flow thickness and velocity parameters because the down-slope spatial variability will depend on levee slope and levee surface resistance. Thus, the equations for mean flow thickness and velocity (Eqns. 7 and 8) should not be considered accurate estimates because they incorrectly assumed terminal flow conditions had been met. The data shown on Figures 4 and 5 can serve as flow thickness and velocity guidelines for smooth slopes until such time that predictive equations are developed.

### **Estimation of Shear Stress**

The most general expression for hydrodynamic shear stress on a slope is given by Eqn. 16 below (Sturm, 2001). This equation is appropriate for unsteady, non-uniform flows on a plane slope that have both convective and temporal accelerations. Shear stresses resulting from combined wave overtopping and steady overflow must be evaluated using Eqn. 16.

$$\tau_0 = \gamma_w h \left[ \sin \theta - \frac{\partial h}{\partial s} - \frac{\partial}{\partial s} \left( \frac{v^2}{2g} \right) - \frac{1}{g} \frac{\partial v}{\partial t} \right] \quad (\text{Unsteady, non-uniform flow}) \quad (16)$$

Steady overflow without waves does not change with time (ignoring turbulent fluctuations), so the temporal acceleration term can be discarded leaving Eqn. 17 for steady, non-uniform flow. This equation accounts for convective accelerations on the landward-side slope in the region that is up-slope from the location where terminal velocity is reached. Note that Nadal and Hughes (2009) mistakenly did not include the down-slope variation of velocity in this equation, so their estimates for steady, non-uniform flow were incorrect.

$$\tau_0 = \gamma_w h \left[ \sin \theta - \frac{\partial h}{\partial s} - \frac{\partial}{\partial s} \left( \frac{v^2}{2g} \right) \right] \quad (\text{Steady, non-uniform flow}) \quad (17)$$

Farther down the slope where the steady overflow has reached terminal velocity, there is no acceleration, and the expression for shear stress simplifies to Eqn. 18 for steady, uniform flow.

$$\tau_0 = \gamma_w h \sin \theta \quad (\text{Steady, uniform flow}) \quad (18)$$

Estimation of hydrodynamic shear stress requires synoptic time series measurements of instantaneous flow thickness and flow velocity at two locations on the landward-side slope. Denoting the up-stream location as position 1 and the down-stream location as position 2, Eqns. 16, 17, and 18 can be represented by discrete versions given by Eqns. 19, 20, and 21, respectively.

$$\tau_0 = \gamma_w \left( \frac{h_2 + h_1}{2} \right) \cdot \left[ \sin \theta - \frac{h_2 - h_1}{s_{2,1}} - \left( \frac{v_2^2 - v_1^2}{2g(s_{2,1})} \right) - \left( \frac{[v_2(i) - v_2(i+1)] + [v_1(i) - v_1(i+1)]}{2g[t(i) - t(i+1)]} \right) \right] \quad (19)$$

$$\tau_0 = \gamma_w \left( \frac{h_2 + h_1}{2} \right) \left[ \sin \theta - \frac{h_2 - h_1}{s_{2,1}} - \left( \frac{v_2^2 - v_1^2}{2g(s_{2,1})} \right) \right] \quad (20)$$

$$\tau_0 = \gamma_w \left( \frac{h_2 + h_1}{2} \right) [\sin \theta] \quad (21)$$

where:

- $h_1$  = Flow thickness at up-stream location
- $h_2$  = Flow thickness at down-stream location
- $s_{2,1}$  = Distance along slope between up-stream and down-stream locations
- $v_1(i)$  = Velocity at up-stream location
- $v_2(i)$  = Velocity at down-stream location
- $v_1(i+1)$  = Velocity at up-stream location, one time increment later
- $v_2(i+1)$  = Velocity at down-stream location, one time increment later
- $t(i)$  = Time at increment  $i$
- $t(i+1)$  = Time at increment  $i+1$

### Estimation of Mean Shear Stress Between Locations P4 and P7

#### STEADY OVERFLOW

Steady, non-uniform overflow shear stresses were estimated using measured time series of flow thickness and velocity acquired at the initial portion of each test when only steady overflow occurred. Shear stress estimates were calculated using Eqn. 20. The calculated time series of steady overflow shear stress was averaged to determine the mean shear stress for each experiment, and this mean represented the average shear stress occurring over the spatial distance separating the up-stream and down-stream measurement locations. Results are listed in Table 2. Estimates were not available for the tests having the lowest surge level because velocity was not measured during the steady overflow portion of the tests. The listed value for  $q_s$  in Table 2 is the average of the values given in Table 1 for P4 and P7. The calculated mean shear stresses strictly represent the average shear stress over the 4.8-m section (prototype scale) of the landward-side slope starting at a distance 2.3 m down from the levee crest and ending at a location 7.1 m down from the levee crest.

Mean shear stress estimates were also calculated using Eqn. 21 which provides a conservative estimate of maximum shear stress  $[(\tau_{o,mean})_{max}]$  would be expected under the same overflow conditions farther down the slope where terminal velocity occurs. These estimates, listed in

Table 2, are conservative because values of mean flow thickness used in Eqn. 21 were larger than the flow thickness that would occur at terminal flow.

Empirical correlations were sought that linked the calculated mean shear stresses to the overflow discharge. The best correlation for the mean shear stress between locations P4 and P7 is shown on Figure 6. The best-fit equation, shown by the solid line in Figure 6, is given by Eqn. 22 below. This equation had a correlation coefficient of 0.924 and an RMS-percent error of 0.0.86. Equation 22 is dimensionally consistent, and it can be used with either SI or English units.

$$\tau_{0,mean} = 0.106 \gamma_w \left( \frac{q_s^2}{g} \right)^{1/3} \quad (\text{Between P4 and P7}) \quad (22)$$

Strictly, the empirical correlation given by Eqn. 22 is only applicable to landward-side slopes having slopes of 1V:3H and similar roughness as the laboratory model, and these equations provide mean shear stress estimates for sections of the landward-side slope where the steady overflow has not yet reached terminal velocity.

An analysis of the ratio of mean shear stress to estimates of the maximum mean shear stress at terminal velocity yielded a simple estimate for maximum mean shear stress given by

$$\left( \tau_{0,mean} \right)_{\max} = 1.41 \tau_{0,mean} \quad (23)$$

with  $\tau_{0,mean}$  calculated using Eqn. 22. As mentioned, the estimate of maximum shear stress is conservative. Nevertheless, for steady overflow, Eqn. 22 should provide reasonable first estimates of actual mean shear stresses that occur over the portion landward-side slope between 2.3 and 7.1 m down from the crest, and Eqn. 23 should give a conservative estimate of the maximum mean shear stress farther down the slope where terminal velocity is reached. It is important to remember that these equations do not apply for landward-side slopes different than 1V:3H or roughness significantly different than the smooth laboratory slope.

#### *COMBINED WAVE AND SURGE OVERTOPPING*

Wave overtopping combined with steady overflow is unsteady in time and non-uniform over distance. The time series of instantaneous shear stresses for combined overtopping were calculated using measured time series of flow thickness and velocity acquired from when

waves first arrived at the levee until the end of the experiment. Shear stress estimates were calculated using Eqn. 19, which is the discrete version of Eqn. 16. It was necessary to employ a filter to remove unrealistically large shear stress spikes due to errant velocity measurements. The filter removed the temporal acceleration term if velocity at the up-stream location was larger than the downstream location and/or shear stress increased more than 2,000 N/m<sup>2</sup> over a 0.05 second span (prototype scale).

The calculated time series of unsteady shear stress was averaged to determine the mean shear stress for each experiment, and this mean represented the average shear stress occurring over the spatial distance between the up-stream and down-stream measurement locations. Table 2 lists the combined overtopping mean shear stresses for the 25 experiments. All time series values have been scaled to prototype size using the length scale  $N_L = 25$  to give a better sense of magnitudes relative to an actual levee. Table 2 also lists maximum mean shear stress estimates that were calculated using Eqn. 21. As noted previously, these maximum estimates are conservative, and they are greater than what would be expected under the same overflow conditions farther down the slope where terminal velocity occurs. Just as for the steady overflow results, the calculated mean shear stresses strictly represent the average shear stress over the 4.8-m length (prototype scale) of the landward-side slope starting at a distance 2.3 m down from the levee crest and ending at a location 7.1 m down from the levee crest.

Empirical correlations were sought that linked the calculated mean shear stresses to the combined overtopping discharge-related parameters. The best correlation, shown in Figure 7, related mean shear stress to the root-mean-square of the individual wave discharge peaks,  $Q_{p,rms}$ . The best-fit equation determined from the shear stress test series for the mean shear stress between locations P4 and P7 is given by Eqn. 24. This equation, shown by the solid line on Figure 7, had a correlation coefficient of 0.914 and an RMS-percent error of 0.095.

$$\tau_{0,mean} = 0.104 \gamma_w \left( \frac{Q_{p,rms}^2}{g} \right)^{1/3} \quad \text{(Between P4 and P7)} \quad (24)$$

where the root-mean-square of the individual wave discharge peaks was given by Hughes and Shaw (2011) as

$$\frac{Q_{p,rms}}{q_{ws}} = 1 + 4.18 \exp \left[ -1.56 \left( \frac{-R_c}{H_{m0}} \right)^{0.88} \right] \quad \text{for } (R_c < 0) \quad (25)$$

The correlation did not include the 7 tests at the lowest surge level because values of  $R_c$  could not be determined, and thus,  $Q_{p,rms}$  could not be calculated. Equations 24 and 25 are dimensionally consistent, and it can be used with either SI or English units. Note that Eqn. 24 is nearly identical to Eqn. 22 for steady overflow with the exception that the discharge parameter is the root-mean-squared value of the shear stress peaks instead of the steady overflow discharge. Because the value of  $Q_{p,rms}$  is the same everywhere on the landward-side slope for a given condition (Hughes and Shaw 2011), the numeric coefficient in Eqn. 24 must be a function of spatial position on the slope. Thus, Eqn. 24 is strictly the average shear stress over the 4.8-m length of levee slope between measurements locations, and the equation is applicable only to landward-side slopes having slopes of 1V:3H and similar roughness as the laboratory model.

An analysis of the ratio of mean shear stress to estimates of the maximum mean shear stress at terminal velocity yielded a simple estimate for maximum mean shear stress given by

$$\left(\tau_{0,mean}\right)_{\max} = 1.42 \tau_{0,mean} \quad (26)$$

with  $\tau_{0,mean}$  calculated using Eqn. 24. As mentioned, the estimate of maximum shear stress is conservative.

### **Estimation of Peak Shear Stress Parameters Between Locations P4 and P7**

Nadal and Hughes (2009) observed that the mean shear stress values estimated for combined wave and surge overtopping provide an overall average that occurs during a combined overtopping event. However, in the time series of instantaneous shear stress acting on the landward-side slope, the peak stresses associated with the overtopping wave crests can be several times the magnitude of the mean shear stress. The peak shear stress acts for a short duration as the wave passes down the slope, but the peak shear stress may be the defining parameter with respect to stability of rapidly-placed protection alternatives or for determining rates of soil erosion.

The calculated time series of instantaneous shear stress from all 25 experiments were analyzed in the time domain using standard up-crossing analysis. The maximum shear stress values for each identified wave were rank-ordered, and representative values were determined for the average of the highest 1/3, highest 1/10, and highest 1/100 of the peak

shear stresses. These values were denoted as  $\tau_{p,1/3}$ ,  $\tau_{p,1/10}$ , and  $\tau_{p,1/100}$ , respectively. Results are tabulated in the three rightmost columns in Table 2.

Good correlations were found between the representative peak shear stresses and the mean shear stress estimated by Eqn. 24. The resulting best-fit correlations are shown on Figure 8 for  $\tau_{p,1/3}$ , Figure 9 for  $\tau_{p,1/10}$ , and Figure 10 for  $\tau_{p,1/100}$ . Notice the high magnitudes of peak shear stress on the ordinate axis compared to the mean values given on the abscissa, and also note that scatter about the central trend increases for the larger representative shear stress parameters.

The solid lines on Figures 8 through 10 are the best-fit linear equations forced through the origin which are provided by Eqns. 27 through 29 below with correlation coefficients of 0.964, 0.925, and 0.865, respectively.

$$\tau_{p,1/3} = 1.64 \tau_{0,mean} \quad (27)$$

$$\tau_{p,1/10} = 2.30 \tau_{0,mean} \quad (28)$$

$$\tau_{p,1/100} = 3.35 \tau_{0,mean} \quad (29)$$

Estimation of the peak shear stress parameters ( $\tau_{p,1/3}$ ,  $\tau_{p,1/10}$ , and  $\tau_{p,1/100}$ ) requires an estimation of the mean shear stress,  $\tau_{0,mean}$ , using an estimated value of  $Q_{p,rms}$ . Each of these empirical equations represents a central trend with data scatter about the trend. Therefore, the combination of multiple empirical equations to estimate the peak shear stress parameters could introduce a cumulative error that might degrade the resulting estimates. This possibility was tested in Hughes, et al. (2011) by comparing calculated peak shear stress values based on measurements to shear stress values estimated using the empirical equations. The comparison is shown on Figure 11 for all 25 experiments. The solid black line in Figure 11 is the line of equivalence. Generally, the empirical equations provided reasonably good predictions with the poorest comparison (understandably) for  $\tau_{p,1/100}$ . The conclusion is that cumulative error from the empirical equations does not have a significant effect on the quality of the peak shear stress estimates.

## CONCLUSIONS

Small-scale, two-dimensional flume experiments with a nominal prototype-to-model length scale of 25 simulated combined wave overtopping and storm surge overflow on a trapezoidal levee cross section. During 27 experiments time series measurements were made of instantaneous flow thickness and velocity at two locations on the levee landward-side slope separated by a distance of about 4.8 m in prototype-scale units. Flow thickness was measured perpendicular to the levee slope, and velocity was measured parallel to the levee slope. The purpose of the experiments was to develop estimates of average and peak shear stresses acting on the landward-side levee slope during combined wave and surge overtopping events associated with a broad range of wave conditions and negative freeboard.

Time series measurements of instantaneous flow thickness and velocity at two locations on the landward-side levee slope revealed that average velocities increased between the two locations whereas average flow thickness decreased. These differences were due to flow acceleration between measurement locations. Estimates of average overtopping discharge at the two measurement locations were well predicted by a previous empirical formulation given by Hughes and Nadal (2009).

Shear stress time series estimates were based on the measured time series of flow thickness and velocity at the two locations on the landward-side slope. For steady overflow shear stress was estimated using the formulation for steady, non-uniform flow on a slope that included the convective acceleration terms. Once waves also begin to overtop the levee, it was necessary to include the temporal acceleration term in the shear stress calculation. These values of instantaneous shear stress represented the average shear stress over the 4.8-m length (prototype scale) of levee slope between the two measurement locations.

A simple empirical equation was proposed for steady overflow that related the mean shear stress to the specific weight of water and the steady discharge. A similar empirical equation was developed for the mean shear stress caused by combined wave overtopping and surge overflow. For the combined overtopping case, mean shear stress was found to be a function of the root-mean-square of the individual overtopping discharge peaks. Conservative estimates for the maximum mean shear stress associated with terminal flow conditions were found to be about 40% greater than the estimated mean shear stress. The more extreme shear stress peaks representing the average of the highest 1/3, 1/10, and 1/100 of the peaks were

found to be linearly related to the estimated mean shear stress. The average of the highest 1/100 peaks was about 3.3 times the mean shear stress.

The predictive equations given in this paper are strictly only applicable for levees having landward-side slopes of 1V:3H with similar slope roughness as the laboratory model. Also the mean shear stress estimates represent an average over the region of the landward-side slope beginning a distance of 2.3 m from the levee crest and ending a distance of 7.1 m from the crest. At some location farther down the levee slope, the flow will reach terminal velocity if the slope length is sufficiently long.

### **ACKNOWLEDGEMENTS**

The research described and the results presented herein, unless otherwise noted, were obtained with support from the research project titled Increasing Community Disaster Resilience Through Targeted Strengthening of Critical Infrastructure at Mississippi State University under project number 70015 and principal investigator Isaac L. Howard. The project was funded by the U.S. Department of Homeland Security through the Southeast Regional Research Initiative (SERRI). Permission was granted by Headquarters, U.S. Army Corps of Engineers, to publish this information. Special thanks to Hugh Acuff, Julie Cohen, and Tim Nisley for their careful and critical support of the laboratory experiments.

**LIST OF SYMBOLS**

$g$	Gravitational acceleration [m/s <sup>2</sup> ]
$H_{m0}$	Energy-based significant wave height [m]
$H_{rms}$	Root-mean-square slope-perpendicular wave height on landward-side slope [m]
$h$	Instantaneous flow thickness [m]
$h_1$	Instantaneous flow thickness at up-stream location [m]
$h_2$	Instantaneous flow thickness at down-stream location [m]
$h_m$	Mean flow thickness [m]
$h_{rms}$	Root-mean-square of the peak flow thickness on the landward-side slope [m]
$L_{om-1,0}$	Wave length associated with mean wave energy [m]
$N_L$	Prototype-to-model length scale [-]
$P1$	Pressure gauge number 1 [-]
$P2$	Pressure gauge number 2 [-]
$P3$	Pressure gauge number 3 [-]
$P4$	Pressure gauge number 4 [-]
$P5$	Pressure gauge number 5 [-]
$P6$	Pressure gauge number 6 [-]
$P7$	Pressure gauge number 7 [-]
$p$	Pressure [kPa]
$Q_{p,rms}$	Root-mean-square of discharge peaks per unit length [m <sup>3</sup> /s/m]
$q$	Instantaneous overtopping discharge per unit length [m <sup>3</sup> /s/m]

$q_s$	Steady overflow discharge per unit length [ $\text{m}^3/\text{s}/\text{m}$ ]
$q_{surge}$	Steady overflow discharge per unit length due to surge [ $\text{m}^3/\text{s}/\text{m}$ ]
$q_{wave}$	Average wave-only overtopping discharge per unit length [ $\text{m}^3/\text{s}/\text{m}$ ]
$q_{ws}$	Average combined wave-surge overtopping discharge per unit length [ $\text{m}^3/\text{s}/\text{m}$ ]
$R_c$	Crest freeboard [m]
$S_f$	Friction slope (slope of the energy-grade line) [-]
$S_0$	Friction slope at steady flow terminal velocity = $\sin\theta$ [-]
$s$	Coordinate parallel to the landward-side levee slope [m]
$s_{2,1}$	Distance along slope between up-stream and down-stream locations [m]
$T_{m-1,0}$	Mean spectral energy wave period [s]
$T_p$	Peak spectral wave period [s]
$t$	Time [s]
$t(i)$	Time at interval $i$ [s]
$t(i+1)$	Time at interval $i+1$ [s]
$v$	Instantaneous velocity parallel to levee surface [m/s]
$v_1(i)$	Instantaneous velocity at up-stream location [m/s]
$v_2(i)$	Instantaneous velocity at down-stream location [m/s]
$v_1(i+1)$	Instantaneous velocity at up-stream location , one time increment later [m/s]
$v_2(i+1)$	Instantaneous velocity at down-stream location, one time increment later [m/s]
$v_m$	Mean velocity on the landward-side slope [m/s]

$\alpha$	Seaward levee slope angle [deg]
$\gamma_w$	Specific weight of water [kN/m <sup>3</sup> ]
$\theta$	Landward-side levee slope angle [deg]
$\xi_{om-1,0}$	Iribarren number based on deepwater wave length and mean energy period [-]
$\pi$	Mathematical pi
$\tau_0$	Instantaneous shear stress [N/m <sup>2</sup> ]
$\tau_{0,mean}$	Mean shear stress [N/m <sup>2</sup> ]
$(\tau_{0,mean})_{max}$	Maximum mean shear stress at terminal velocity [N/m <sup>2</sup> ]
$\tau_{p,1/3}$	Average of highest 1/3 shear stress peaks [N/m <sup>2</sup> ]
$\tau_{p,1/10}$	Average of highest 1/10 shear stress peaks [N/m <sup>2</sup> ]
$\tau_{p,1/100}$	Average of highest 1/100 shear stress peaks [N/m <sup>2</sup> ]

## REFERENCES

- Briaud, J.-L., Chen, H.-C., Govindasamy, A. V., and Storesund, R. 2008. "Levee erosion by overtopping in New Orleans during the Hurricane Katrina. *Journal of Geotechnical and Geoenvironmental Engineering*, American Society of Civil Engineers, Vol 134, No. 5, pp 618-632.
- Gibson, A. H. 1930. "The effect of surface waves on the discharge over weirs," *The Institution of Civil Engineers*, London, Paper No. 99, pp 1-18.
- Goda, Y., and Y. Suzuki. 1976. "Estimation of incident and reflected waves in random wave experiments," *Proceedings 15th International Coastal Engineering Conference*, American Society of Civil Engineers, Vol 1, pp 828-845.
- Henderson, F. M. 1966. *Open channel flow*, MacMillian Publishing Co., New York.
- Hughes, S.A. 2008. "Combined wave and surge overtopping of levees: Flow hydrodynamics and articulated concrete mat stability" Technical Report ERDC/CHL TR-08-10, U.S. Army Engineer Research and Development Center, Vicksburg, MS.
- Hughes, S. A., and Nadal, N. C. 2009. "Laboratory study of combined wave overtopping and storm surge overflow of a levee," *Coastal Engineering*, Elsevier, Vol 56. No. 3, pp 244-259.
- Hughes, S. A., and Nadal, N. C. 2010. "Flow parameters of combined wave overtopping and storm surge overflow of a trapezoidal levee," *Proceedings of Coasts, Marine Structures and Breakwaters: 9th International Breakwaters Conference 2009*, Institution of Civil Engineers, London, Vol 2, pp 562-573.
- Hughes, S. A., and Shaw, J. M. 2011. Continuity of instantaneous overtopping discharge with application to stream power concepts. *Journal of Waterway, Port, Coastal, and Ocean Engineering*, American Society of Civil Engineers, Vol 137, No. 1, pp 12-25.
- Hughes, S. A., Sharp, J. A., Shaw, J. M., Howard, I. L., and McAnally, W. H. 2011. "Physical testing and hydraulic simulation of wave overtopping of earthen levees," SERRI Report 70015-008, Oak Ridge National Laboratory, Oak Ridge, TN (in press).

Losada, I. J., Lara, J. L., Guanche, R., and Gonzalez-Ondina, J. M. 2008. "Numerical analysis of wave overtopping of rubble mound breakwaters, *Coastal Engineering*, Elsevier, Vol 55. No. 1, pp 47-62.

Lynett, P. J., Melby, J. A., and Kim, D-H. 2010. "An application of Boussinesq modeling to Hurricane wave overtopping and inundation," In: Demirbilek (editor), Special issue of Ocean Engineering, Elsevier, Vol 37, pp 135-153.

Nadal, N. C., and Hughes, S. A. 2009. "Shear stress estimates for combined wave and surge overtopping at earthen levees." Coastal and Hydraulics Engineering Technical Note ERDC/CHL CHETN-III-79, U.S. Army Engineer Research and Development Center, Vicksburg, MS.

Pullen T., Allsop, N.W.H., Bruce, T., Kortenhaus A., Schüttrumpf H., van der Meer, J. W. 2007. "EurOtop: Wave overtopping of sea defences and related structures: Assessment Manual," [www.overtopping-manual.com](http://www.overtopping-manual.com).

Reeve, D. E., Soliman, A., and Lin, P. Z. 2008. "Numerical study of combined overflow and wave overtopping over a smooth impermeable seawall," *Coastal Engineering*, Elsevier, Vol 55, pp 155-166.

Schüttrumpf, H. 2001. Wellenüberlaufströmung bei Seedeichen – Experimentelle und Theoretische Untersuchungen. PhD-Thesis.

Schüttrumpf, H., Möller, J., and Oumeraci, H., Grüne, J., and Weissmann, R. 2001. "Effects of natural sea states on wave overtopping of seadikes," *Proceedings of the 4th International Symposium Waves 2001, Ocean Wave Measurement and Analysis*, American Society of Civil Engineers, Vol 2, pp 1565-1574.

Sturm, T.W. 2001. *Open channel hydraulics*. McGraw-Hill, New York, NY.

van der Meer, J. W., Bernardini, P., Snijders, W., and Regeling, E. 2006. "The wave overtopping simulator," *Proceedings of the 30th International Conference on Coastal Engineering*, World Scientific, Vol 5, pp 4654-4666.

van der Meer, J. W., Steendam, G. J., de Raat, G., and Bernardini, P. 2008. "Further developments on the wave overtopping simulator," *Proceedings of the 31st International*

*Conference Coastal Engineering*, American Society of Civil Engineers, Vol 4, pp. 2957-2969.

van der Meer, J. W., Hardeman, B., Steendam, G. J., Schüttrumpf, H., and Verheij, H. 2010. "Flow depths and velocities at crest and inner slope of a dike, in theory and with the wave overtopping simulator," *Proceedings of the 32st International Conference Coastal Engineering*, American Society of Civil Engineers, (in press).

### **Table Captions**

Table 1. Mean overtopping discharge (prototype scale)

Table 2. Root-mean-squared difference between discharge time series at locations P2 and P6.

### **Figure Captions**

Figure 1. Cross section of model levee.

Figure 2. Measurement locations on levee model cross section.

Figure 3. Laser Doppler velocimeters positioned for measurements.

Figure 4. Mean combined overtopping flow thickness (prototype scale).

Figure 5. Mean combined overtopping flow velocity (prototype scale).

Figure 6. Surge overflow mean shear stress as a function of discharge (prototype scale).

Figure 7. Combined overtopping mean shear stress as a function of  $Q_{p,rms}$  (prototype scale).

Figure 8. Average of highest 1/3 shear stress peaks (prototype scale).

Figure 9. Average of highest 1/10 shear stress peaks (prototype scale).

Figure 10. Average of highest 1/100 shear stress peaks (prototype scale).

Figure 11. Prediction of representative shear stress peaks (prototype scale).

Table 1. Mean overtopping discharge (prototype scale).

Run #	Prototype-Scale Parameters				Position P4		Position P7	
	$H_{mo}$ (m)	$T_p$ (sec)	$T_{m-1,0}$ (sec)	$R_c$ (m)	$q_s$ (m <sup>3</sup> /s/m)	$q_{ws}$ (m <sup>3</sup> /s/m)	$q_s$ (m <sup>3</sup> /s/m)	$q_{ws}$ (m <sup>3</sup> /s/m)
R26	0.92	10.40	8.70	—	—	0.68	—	1.04
R28	1.78	6.02	5.47	—	—	0.97	—	1.25
R29	1.77	10.44	8.72	—	—	1.14	—	1.36
R30	1.78	14.62	10.64	—	—	1.31	—	1.46
R31	2.56	6.02	5.70	—	—	1.22	—	1.34
R32	2.63	10.04	8.81	—	—	1.58	—	1.72
R33	2.58	14.62	9.96	—	—	1.67	—	1.84
R34	0.85	6.02	5.65	-1.12	2.03	2.04	1.83	1.80
R35	0.85	10.04	8.63	-1.12	2.01	2.06	1.80	1.74
R36	0.84	13.85	11.34	-1.08	1.90	1.86	1.99	1.97
R37	1.61	5.88	5.46	-1.10	1.96	2.29	1.89	2.23
R38	1.73	10.04	8.50	-1.13	2.05	2.44	1.93	2.24
R39	1.71	13.85	11.23	-1.13	2.06	2.49	1.83	2.18
R40	2.47	5.88	5.62	-1.09	1.93	2.42	2.02	2.53
R41	2.60	10.04	8.61	-1.11	1.98	2.73	2.07	2.82
R42	2.53	13.85	10.65	-1.03	1.79	2.57	2.45	3.22
R43	0.70	6.02	5.53	-1.59	3.43	3.43	3.46	3.47
R44	0.78	10.04	8.55	-1.60	3.44	3.44	3.41	3.42
R45	0.80	13.12	11.39	-1.60	3.45	3.46	3.33	3.39
R46	1.27	6.02	5.53	-1.61	3.49	3.48	3.38	3.41
R47	1.62	10.04	8.46	-1.62	3.50	3.48	3.36	3.45
R48	1.64	13.12	11.05	-1.62	3.52	3.48	3.38	3.43
R49	2.37	6.02	5.61	-1.63	3.53	3.46	3.40	3.52
R50	2.53	10.04	8.35	-1.62	3.53	4.01	3.46	4.14
R51	2.54	13.85	10.40	-1.65	3.62	4.08	3.69	4.33

Table 2. Mean and peak shear stress parameters between P4 and P7 (prototype scale).

Run	Steady Overflow			Combined Wave and Surge Overtopping					
	Average P4 to P7			Average P4 to P7			Peak Parameters		
	$q_s$ (m <sup>3</sup> /s/m)	$\tau_{0,mean}$ (N/m <sup>2</sup> )	$(\tau_{0,mean})_{max}$ (N/m <sup>2</sup> )	$Q_{p,rms}$ (m <sup>3</sup> /s/m)	$\tau_{0,mean}$ (N/m <sup>2</sup> )	$(\tau_{0,mean})_{max}$ (N/m <sup>2</sup> )	$\tau_{p,1/3}$ (N/m <sup>2</sup> )	$\tau_{p,1/10}$ (N/m <sup>2</sup> )	$\tau_{p,1/100}$ (N/m <sup>2</sup> )
R26	—	—	270	—	838	919	1,573	2,029	2,859
R28	—	—	256	—	1,238	1,135	1,965	2,477	3,305
R29	—	—	224	—	1,333	1,437	2,109	2,701	3,435
R30	—	—	260	—	1,394	1,651	2,393	3,313	4,237
R31	—	—	166	—	1,523	1,412	2,283	2,948	4,451
R32	—	—	252	—	1,765	1,931	2,836	3,962	5,489
R33	—	—	270	—	1,588	2,178	2,877	4,352	7,236
R34	1.93	817	986	3.02	1,129	1,414	1,679	2,333	3,360
R35	1.91	685	977	2.99	1,084	1,474	1,554	2,197	3,193
R36	1.95	718	988	3.06	964	1,464	1,402	1,992	3,311
R37	1.93	694	982	5.36	1,764	1,889	2,862	3,629	4,281
R38	1.99	832	1,015	5.69	1,641	2,177	2,675	3,703	5,218
R39	1.94	925	1,000	5.64	1,627	2,209	2,806	4,020	5,782
R40	1.98	662	996	7.32	2,033	2,319	3,315	4,309	5,675
R41	2.03	796	1,021	8.32	2,140	2,816	3,686	5,326	8,139
R42	2.12	705	1,039	8.86	1,884	2,977	3,439	5,322	8,547
R43	3.44	1,121	1,605	4.03	1,130	1,990	1,331	1,493	1,851
R44	3.42	1,086	1,602	4.19	1,142	2,088	1,346	1,479	1,816
R45	3.39	1,121	1,588	4.24	1,135	2,084	1,345	1,522	1,810
R46	3.44	1,120	1,606	5.55	1,452	2,317	2,115	3,238	4,333
R47	3.43	968	1,609	6.51	1,614	2,715	2,589	3,751	4,548
R48	3.45	1,103	1,621	6.54	1,506	2,725	2,348	3,817	5,662
R49	3.47	1,153	1,622	8.24	2,040	2,927	3,435	4,520	6,133
R50	3.49	1,075	1,636	10.01	1,994	3,637	3,449	5,372	9,656

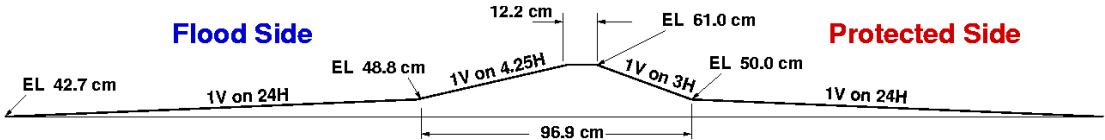


Figure 1. Cross section of model levee.

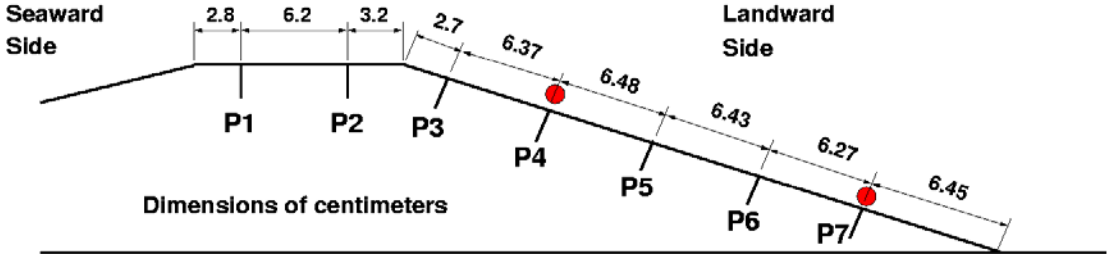


Figure 2. Measurement locations on levee model cross section.



Figure 3. Laser Doppler velocimeters positioned for measurements.

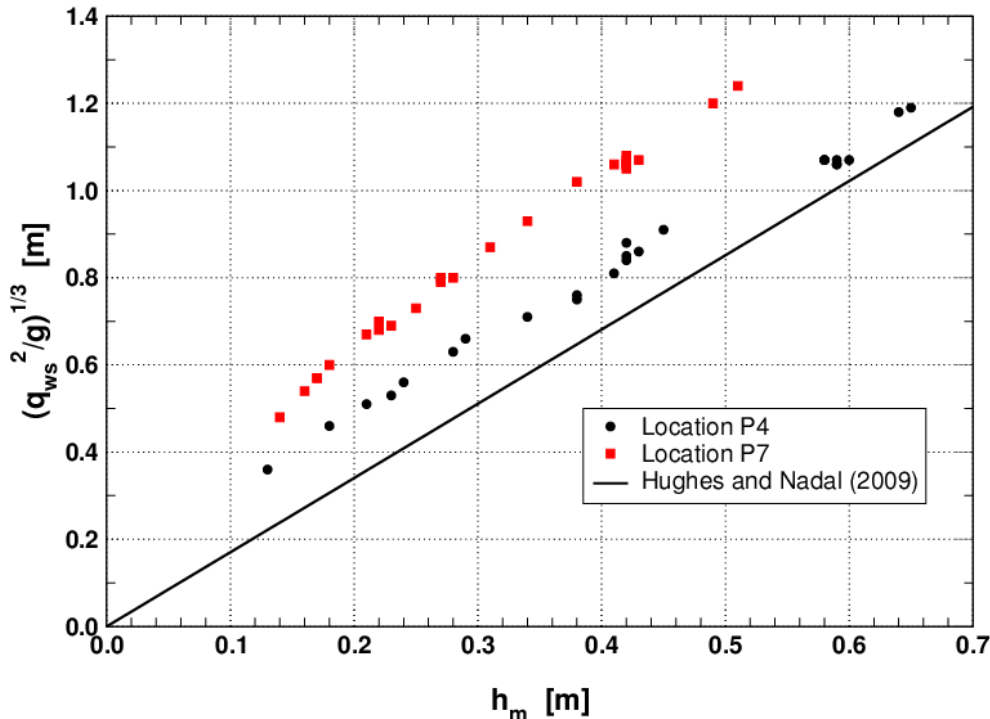


Figure 4. Mean combined overtopping flow thickness (prototype scale).

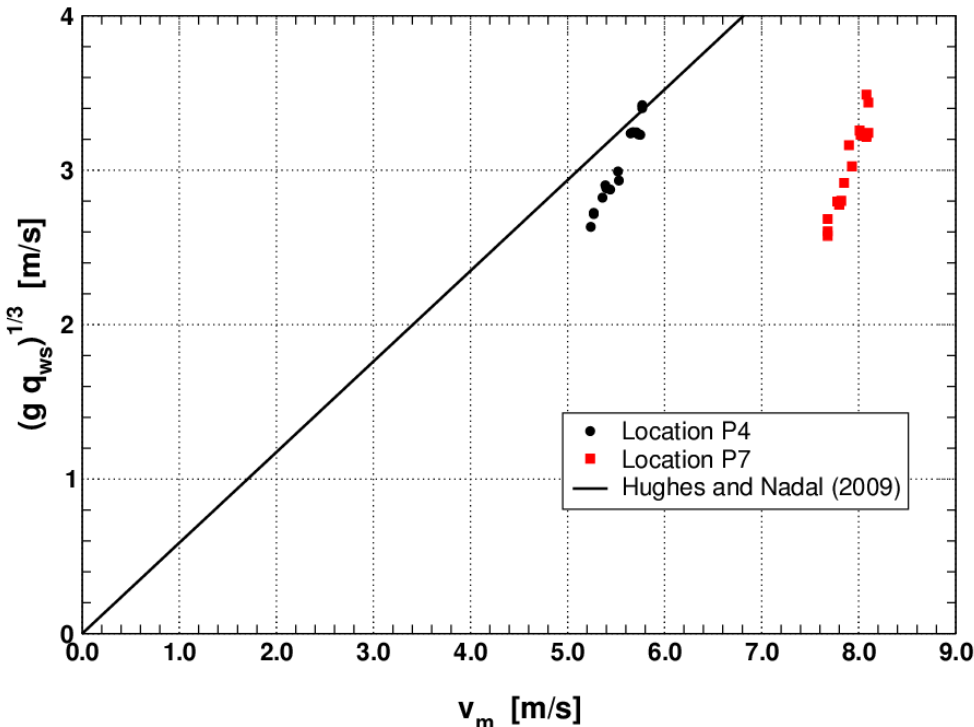


Figure 5. Mean combined overtopping flow velocity (prototype scale).

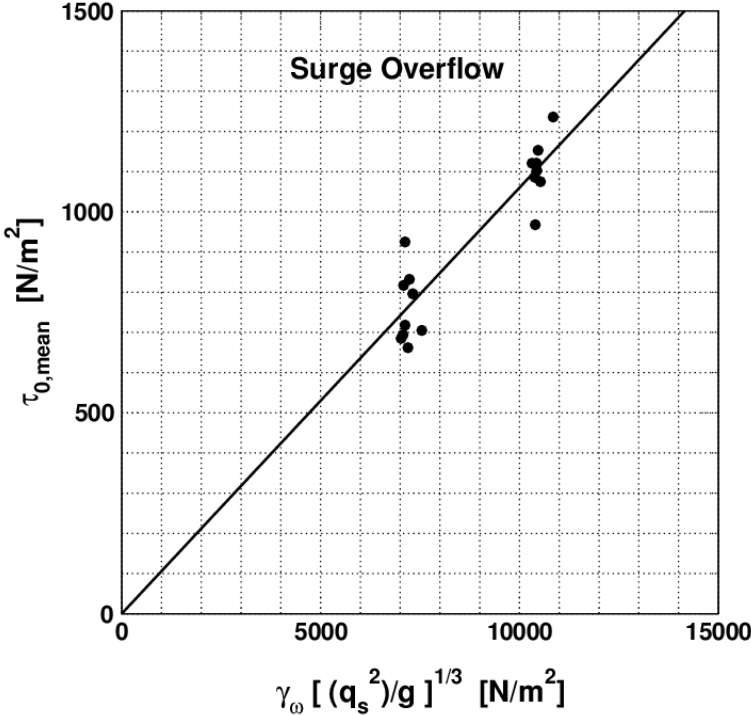


Figure 6. Surge overflow mean shear stress as a function of discharge (prototype scale).

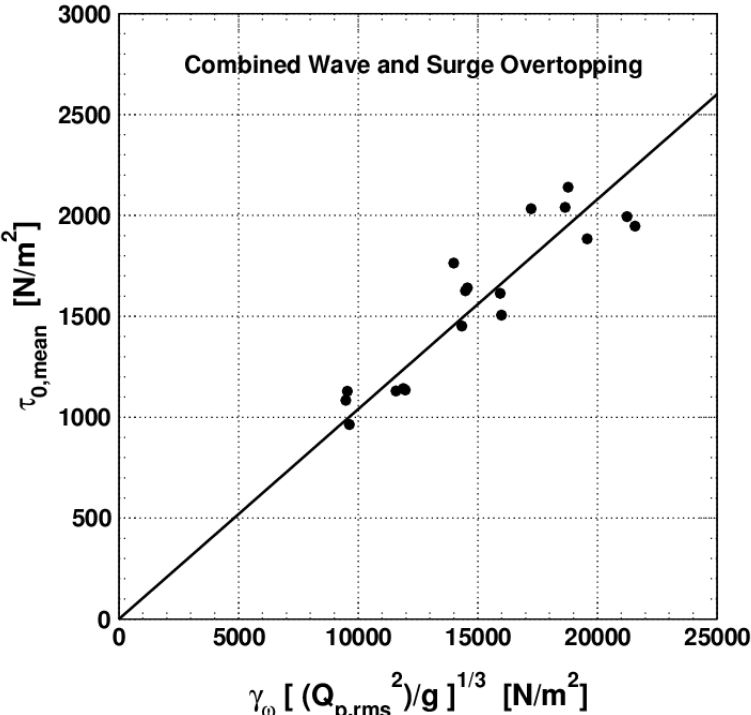


Figure 7. Combined overtopping mean shear stress as a function of  $Q_{p,rms}$  (prototype scale).

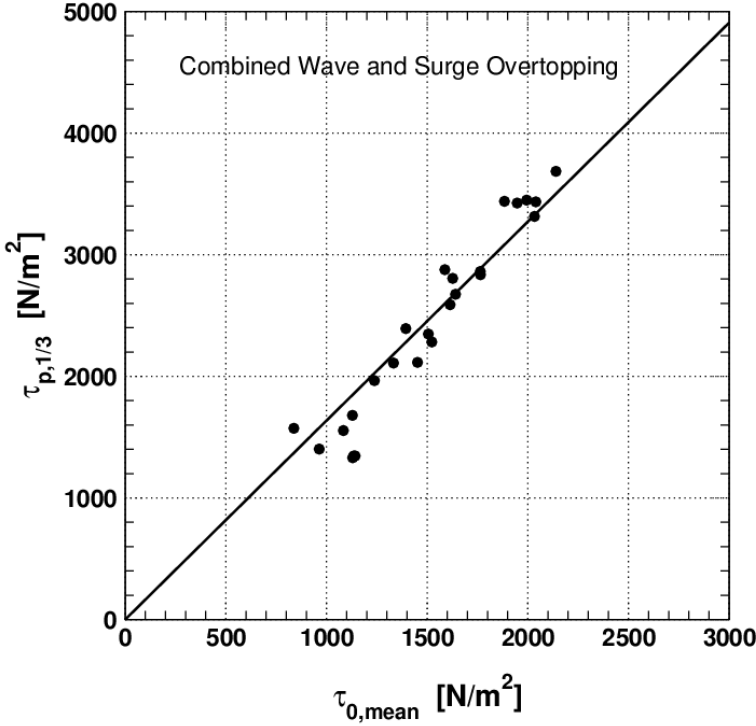


Figure 8. Average of highest 1/3 shear stress peaks (prototype scale).

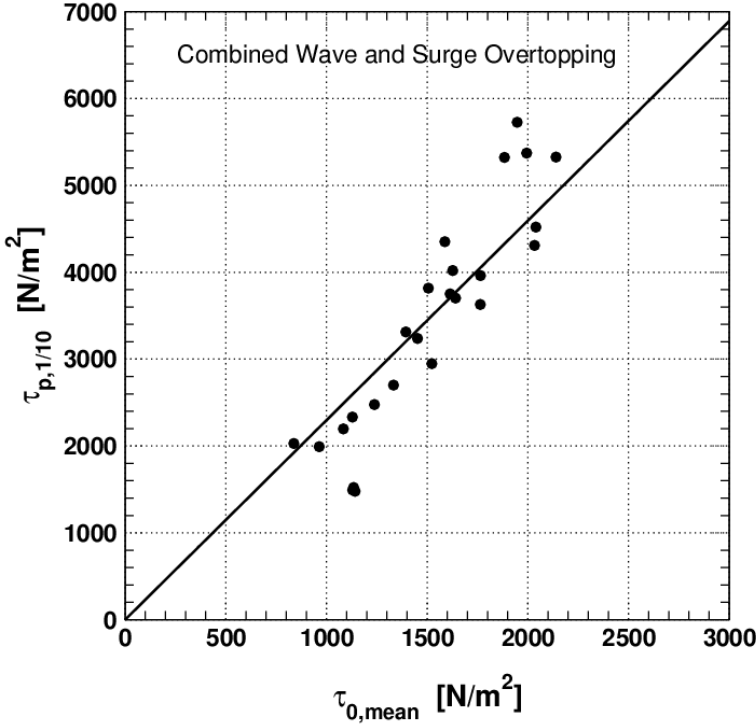


Figure 9. Average of highest 1/10 shear stress peaks (prototype scale).

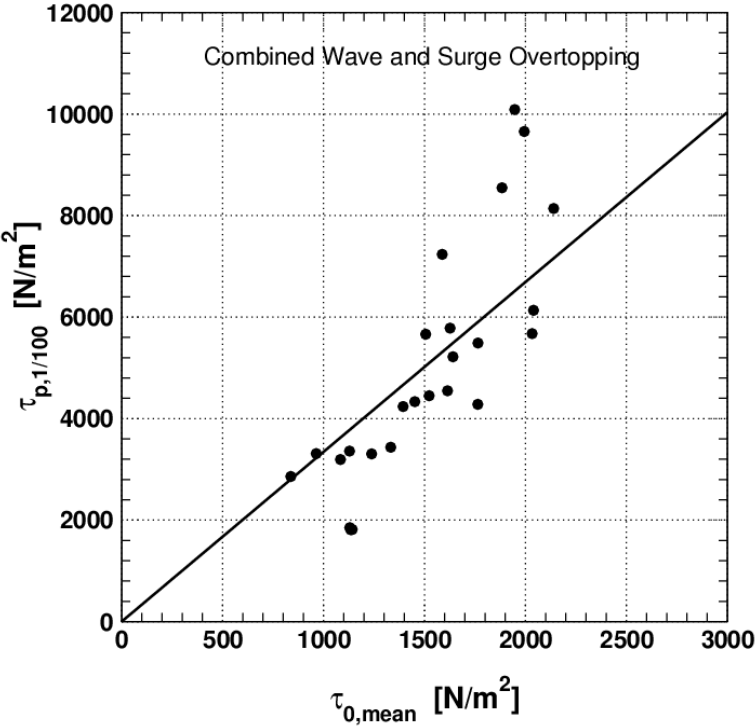


Figure 10. Average of highest 1/100 shear stress peaks (prototype scale).

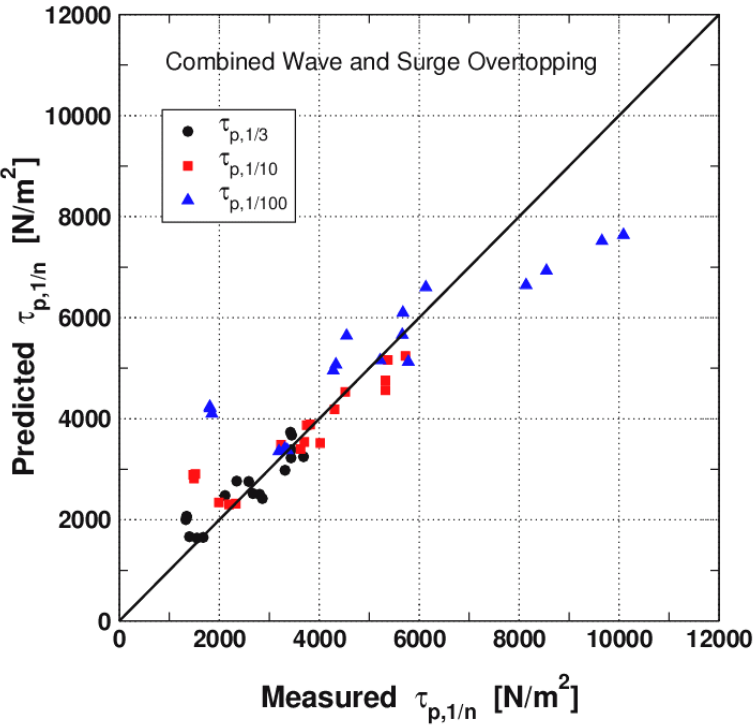


Figure 11. Prediction of representative shear stress peaks (prototype scale).